Proceedings of the 2nd International Conference on Computing Innovation and Applied Physics (CONF-CIAP 2023)
DOI: 10.54254/2753-8818/5/20230337

Long-range and short-range dihadron correlations in central PbPb collisions at $\sqrt{s_{NN}} = 5.02\ TeV$ and centrality 40-50%

Yunfan Bai[1,*], Junzhe Liu[2]

[1]Physics Department, Imperial College London, London, SW7 2AZ, United Kingdom
[2]Valley Christian High School, San Jose, 95111, USA

*Corresponding author's e-mail: ab3921@ic.ac.uk

Abstract: This paper reports the first measurement of charged particle elliptic flow in Pb-Pb collisions at $\sqrt{s_{NN}} = 5.02T\ eV$ with the ALICE detector at the CERN Large Hadron Collider. The measurement is performed on more than 20,000 events in 40-50% centrality class on both long-range $2 < |\Delta\eta| < 4$ and short-range $|\Delta\eta| < 1$ regions. The two-particle correlation method is used over long-range region, in the transverse momentum range of $1 < p_T < 1.5GeV$, and the elliptic flow signals, given by $v_n = \sqrt{V_n}$, are $v_2 = 0.17 \pm 0.01, v_3 = 0.07 \pm 0.01, v_4 = 0.04 \pm 0.01, v_5 = 0.03 \pm 0.01$. Since V_1 is obtained as -0.0013, it does not have a square root value. In addition, for $n = 2 - 4$, it is found that v_n increases as p_T increases. The Q-vectors method is also used to determine the values of v_2. The magnitudes of the Q-vectors are fitted to a function. The values of v_2 produced by the two methods are compared and discussed. At the end, the vectors are used to analyse high-energy jet particles.

Keywords: high energy collisions, hydrodynamic flow, two-particle correlation, Q vector.

1. Introduction

The study of two-dimensional(2D) $\Delta\eta - \Delta\phi$ correlation during relativistic nucleus-nucleus collisions play indispensable role in comprehending the underlying mechanism of evolution of particles during collisions of protons and nuclei of very high energy[1]. Here, $\Delta\phi$ is the difference in azimuthal angle ϕ and $\Delta\eta$ is the difference in pseudorapidity η, which is defined by $-ln(tan(\theta/2))$, between the two collision particles. Early results produced from PbPb collisions in the Large Hadron Collider [1-4] enhanced studies on the dihadron collisions to a higher energy regime, compared to those from the Relativistic Heavy Ion Collider (RHIC) [5-12].

In this paper, the data from a PbPb collision data file is analysed in order to help one characterize the pattern of elliptic flow, a phenomenon that takes place during the collision of heavy ions [13], in this paper's case between two Pb ions, that contributes to the 2D correlation. Due to the asymmetric distribution of interacting nuclei inside each ion, an asymmetric expansion evolves, being faster at the reaction plane, along the direction of the jet, than the plane perpendicular to it. This results in a asymmetric distribution of particles in the azimuthal plane in the final state, which is the so-called elliptic flow.

DOI: 10.54254/2753-8818/5/20230337

Using two methods of simulation of the elliptic flow, the Q-vector method and the two-particles correlation method, and comparing the results, this work aims to numerically determine the equation of the elliptic flow.

In two-particles correlation method, the transverse momentum of the long-range $2 < |\Delta\eta| < 4$ and short-range $|\Delta\eta| < 1$ dihadron correlations are examined seperately. For the long range correlations, particles with transverse momentum in the range of $1 < p_T < 1.5GeV$. In contrast, particles of $p_T > 3GeV$ and $p_T < 1GeV$ are chosen to study the short range correlations, where the second method is not suitable to be applied due to large contribution for jet fragmentation at near side, $\Delta\phi = 0$, and away side, $\Delta\phi = \pi$, that is unrelated to hydrodynamic flow.

The nth harmonic of the event flow vector, Q_n, represents the nth symmetry of the quark-gluon plasma. For example, Q_2 reveals the elliptical component of the plasma while Q_3 corresponds to the triangular component. For the Q-vector method, no systematic selection of flow components is made. However, a term in the curve fit is introduced to account for the non-flow components of the data. In the jet section, $p_T < 2GeV$ is selected for the q_2.

2. Experimental setup

The data file contains about 20,000 events of PbPb collisions of centrality of 40% to 50% at a nucleon center-of-mass energy of $\sqrt{s_{NN}} = 5.02T\ eV$. Each event contains about 300 particles interacting. For each particle, one recorded its transverse momentum p_T, azimuthal angle ϕ, and pseudorapidity η.

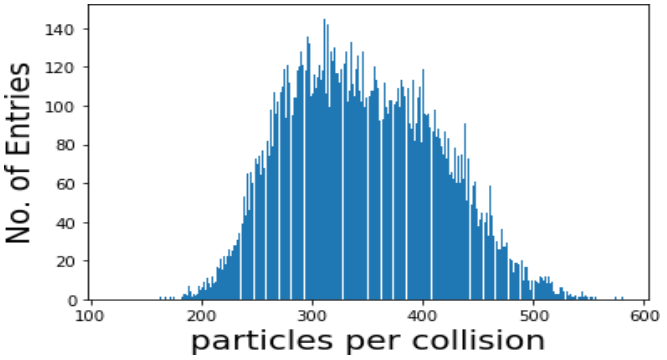

(a)Number of Particles in Each Event

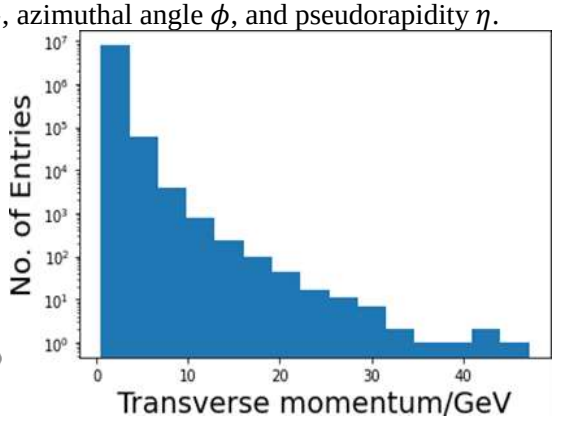

(b)Distribution of pT

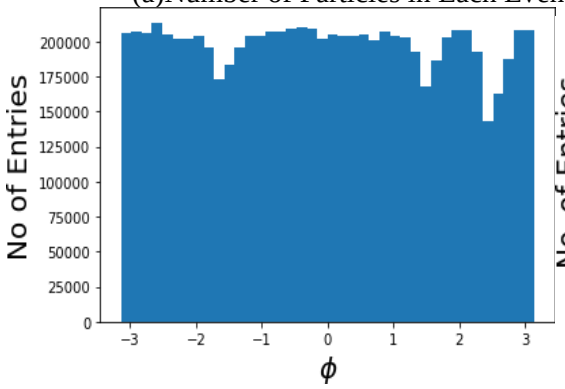

(c)Distribution of ϕ

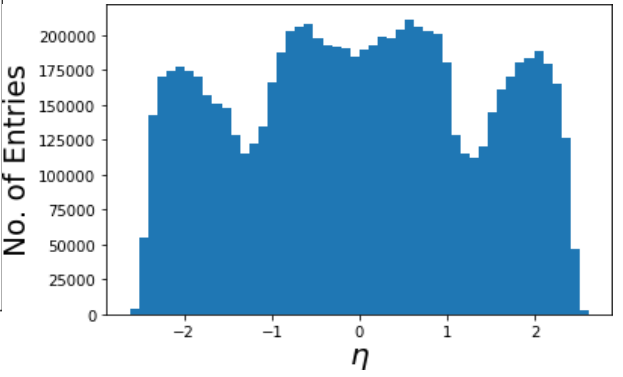

(d) Distribution of η

DOI: 10.54254/2753-8818/5/20230337

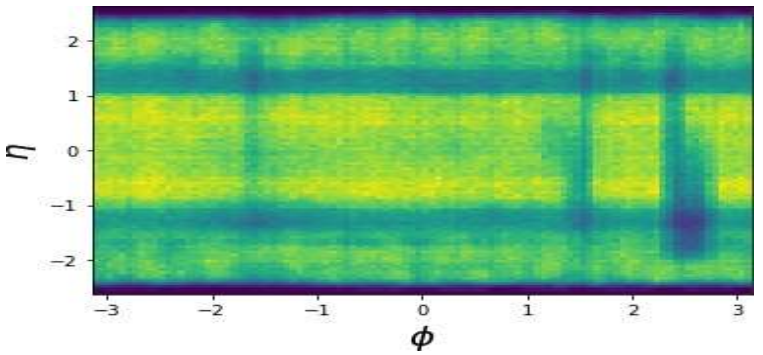

(e) η Against ϕ

Figure 1. Distribution of diverse variables in the data file [Owner-draw].

Figure 1 shows the distribution of different variables contained in the data file. Subfigure1a shows the distribution of number of particles for each event. One observes a normal distribution around 300 particles. Subfigure 1b shows the distribution of p_T in the whole data file, with the y-axis at a logarithmic scale. An exponential decrease can be seen. Subfigure 1c shows the ϕ distribution, which sinks at three points. Subfigure 1d shows a non-uniform distribution of η, which may be dependent on the direction of jet. In addition, a 2D histogram is plotted for the pseudorapidity against the azimuthal angle at Subfigure 1e. The graph shows an overall uniform distribution but has a dark spot at (ϕ, η) of $(2.5,1.25)$ indicating more numbers of entries.

3. Data analysis

3.1. Method to analyze elliptic flow

3.1.1. Two particles correlation. The first Fourier decomposition analysis of long range dihadron azimuthal correlation is applied in [4] for PbPb collisions of $\sqrt{s_{NN}} = 2.76T\ eV$. The same process is applied in this paper. A variety of bins of trigger transverse momentum, p_T^{trig} , are considered. The total number of trigger particles for the whole data file is denoted by N_{trig}. Within each event, each trigger particle is paired with every associated particles binned in p_T^{assoc} . The differential yield of associated particles per trigger particle is

$$\frac{1}{N_{trig}} \frac{d^2 N^{pair}}{d\Delta\phi d\Delta\eta} = B(0,0) \times \frac{S(\Delta\eta, \Delta\phi)}{B(\Delta\eta, \Delta\phi)} \tag{1}$$

where N^{pair} is the total number of correlated hadron pairs. The functions $S(\Delta\eta, \Delta\phi)$ and $B(\Delta\eta, \Delta\phi)$ denote the signal and background distribution respectively. The value of $B(0,0)$ is a normalisation factor that is considered as a fitted constant in this paper. The signal distribution considers pairs of trigger and associated particles in the same event,

$$S(\Delta\eta, \Delta\phi) = \frac{1}{N_{trig}} \frac{d^2 N^{same}}{d\Delta\phi d\Delta\eta} \tag{2}$$

where N^{same} is the number of such pairs within the $(\Delta\eta, \Delta\phi)$ bin. In contrast, the background distribution involves a similar number of trigger and associated pairs of mixed event, that is between 2 or 3 different randomly chosen events.

$$B(\Delta\eta, \Delta\phi) = \frac{1}{N^{trig}} \frac{d^2 N^{same}}{d\Delta\phi d\Delta\eta} \tag{3}$$

where N^{mix} denotes the number of mixed-event pairs. This distribution represents the expected correlation if only the non-uniformity in the distribution of azimuthal angle ϕ is considered.

DOI: 10.54254/2753-8818/5/20230337

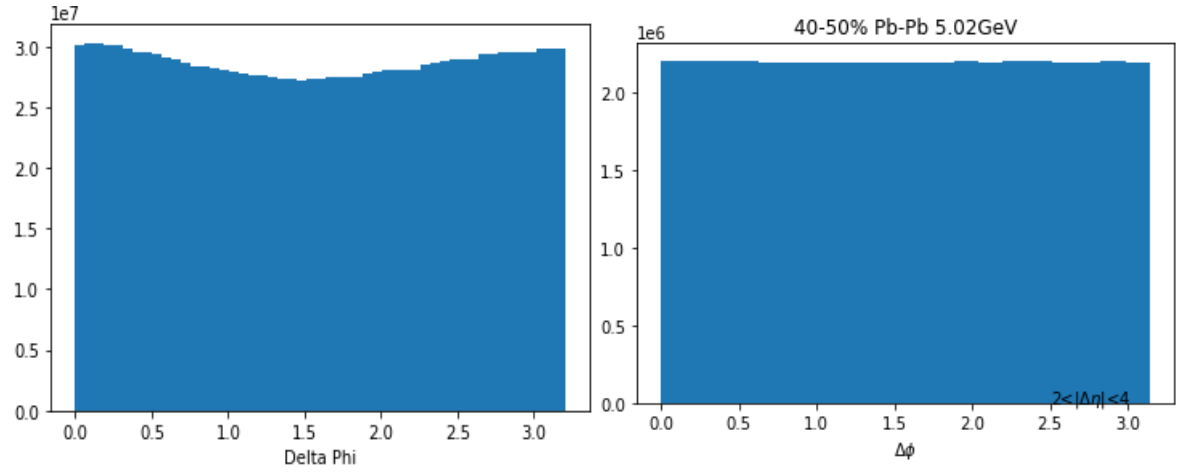

(a) Signal Distribution (b) Background Distribution

Figure 2. The distribution of associated yield separated by Δϕ. The Signal Distribution is from pairs of same event, and the Background Distribution from pairs of different events [Owner-draw].

Figure 2 shows the signal and background distribution of the data file, binned by Δϕ. Subfigure 2a shows the signal distribution of hadron pairs inside the same event for 2 < $|\Delta\eta|$ < 4, while Subfigure 2b shows the background distribution of mixed event. One observes that the signal distribution follows a sinusoidal distribution, whereas $|\Delta\phi|$ of mixed event is uniformly distribution between 0 and π.

The equations for this paper applies the same Fourier Series as in [1-4] to fit the 1D Δϕ distribution

$$\frac{1}{N_{trig}}\frac{dN_{pair}}{d\Delta\phi} = \frac{N_{assoc}}{2\pi}\left\{1 + \sum_{n=1}^{N_{max}} 2V_{n\Delta}\cos(n\Delta\phi)\right\} \tag{4}$$

where $V_{n\Delta}$ are the Fourier coefficients to be fitted and N_{assoc} represents the total number of hadron pairs per trigger particle for the given $\Delta\eta$ range in the $\{p_T^{trig},\ p_T^{assoc}\}$ bin. The first five terms are considered ($N_{max} = 5$).

To begin with, a set of $V_{n\Delta}$ are obtained from fitting the equation to trigger particles and associated particles in the same middle range region of $1 < pT < 1.5GeV$. This is because in this region, the particles are solely affected by the hydrodynamic flow, so the hadron pairs follow exactly the pattern represented by the Eq. 4. The binning of $\Delta\phi$ separates the distribution of associated yield into 20 different bins. A histogram of the $\Delta\phi$ evolved from hadron pairs of the same event is produced with another of $\Delta\phi$ from mixed events. The left hand side value of Eq. 4 can be obtained from dividing the first histogram by the second histogram. In Subfigure 3a, the data points are plotted with the curve of the fitted equation. Absolute error exists for the data points for N^{same} and N^{mix} as $\sqrt{N}$, however, the error bars are smaller than the marker sizes so cannot be observed in the plots. Then, the absolute values of the Fourier coefficients $|Vn\Delta|$ generated are plotted together with a logarithmic y scale to make a comparison in Subfigure b. Statistical error exists in the covariance generated by the curve-fit function of Python, and are drawn as error bars in the graph. The $V_{n\Delta}$s obtained are $V_1 = -0.0013, V_2 = 0.0260, V_3 = 0.0033, V_4 = 0.0008\ and\ V_5 = 0.0005$, each with a statistical error of 0.0002. One finds that the value of $V_{n\Delta}$ peaks at $n = 2$, and drops dramatically as n increases, which agrees with the findings of [4]. The value for $n = 1$ is curiously negative at a value of -0.0013, which is the reason for taking an absolute value. The elliptic flow signals, given by $v_n = \sqrt{V_{n\Delta}}, are\ v_2 = 0.17 \pm 0.01, v_3 = 0.07 \pm 0.01, v_4 = 0.04 \pm 0.01, v_5 = 0.03 \pm 0.01$. Since V_1 is obtained is negative, it does not have a square root value.

DOI: 10.54254/2753-8818/5/20230337

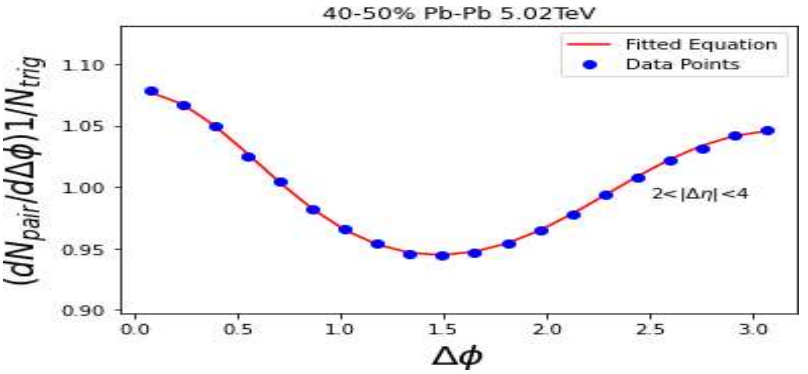

(a) Comparison of fitted equation with data

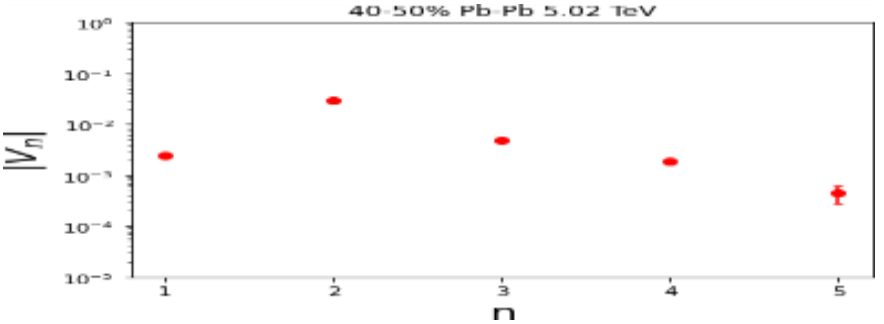

(b) VnΔ

Figure 3. Results for fitting the equation to particles of transverse momentum $1 < p_T < 1.5GeV$.

A similar set of plots are also generated for the high and low p_T ranges of $p_T > 3GeV$ and $p_T < 1GeV$ in Figure 3. However, as shown in Fig.4, the pattern clearly does not solely follow hydrodynamic flow and involves other unknown factors, making this method unsuitable for obtaining accurate result.

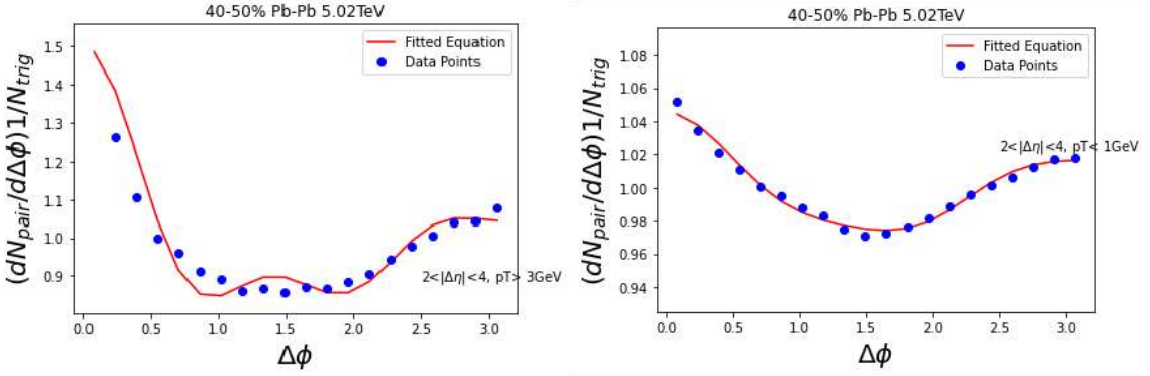

$(a) p_T >$ 3GeV (b) $p_T <$ 1GeV

Figure 4. Results for fitting the equation to particles of transverse momentum $1 < p_T < 1.5GeV$.

Afterwards, the particles in the data file are divided into 10 different bins of p_T^{trig}, each bin containing similar number of particles inside. The interaction between these trigger particles and associated particles of the same bin range is studied. A set of $V_{n\Delta}$ are obtained from the fitted equation for each of the groups, and the $V_{n\Delta}$ are plotted separately against p_T to study their correlation, with the error bars representing the covariance generated by the curve-fit function. Each $V_{n\Delta}$ generated contains a statistical error generated by the curve-fit function of Python, which is plotted as error bar in Fig. 5. It is observed that for n=2,3 and 4, a significant positive relationship can be determined, as V_n increasing with increasing p_T. However, for n=1 and n=5, the statistical error is too big to successfully find a valid relationship.

DOI: 10.54254/2753-8818/5/20230337

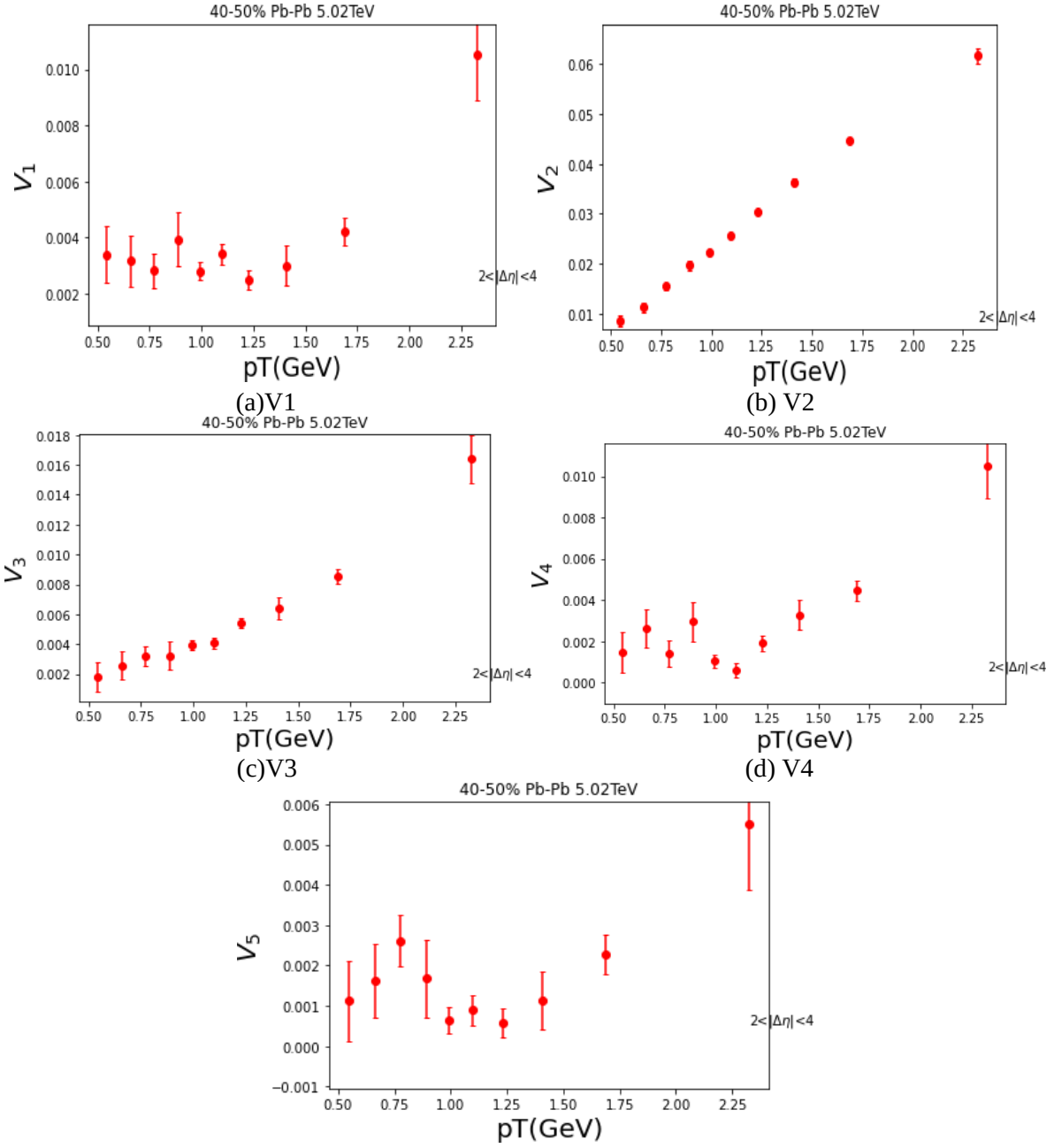

Figure 5. The values of $V_{n\Delta}$ against p_T.

3.1.2. Q-vector. Qn is calculated for each event with

$$Q_n \sin(n\Psi_n) = \sum_i \sin(n\phi_i) \tag{5}$$

$$Q_n \cos(n\Psi_n) = \sum_i \cos(n\phi_i)$$

DOI: 10.54254/2753-8818/5/20230337

where Ψ_n, Q_n defines the direction and magnitude of the flow vector. The magnitude specifies the amount of symmetry; Ψ is the direction where the detected particle frequency is the highest. Thus, when divided by the number of particles in each event, the shape of Q_n distribution should match that of v_n.

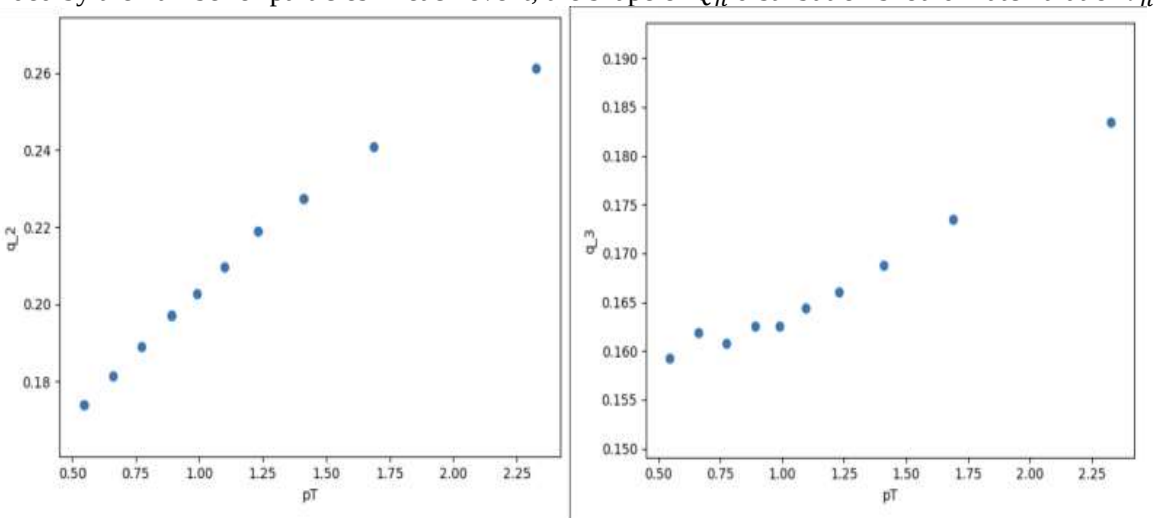

(a)The distribution of $Q2/M$ over the bins of p_T (b)The distribution of $Q3/M$ over the bins of p_T

Figure 6. The Q vectors for each event is calculated then divided by the multiplicity M of the event. Qn/M is then averaged over each bin selection of p_T to produce the data points on the graph.

As shown in Figure 6, the shape of $Q2/M$ and $Q3/M$ distribution corresponds to that of V_2, V_3 in Figure 5. However, the values of the normalized Q vectors are much higher than the corresponding flow coefficient. This discrepancy is caused by the limitation of the Q-vector method: difficulties in making selections in $\Delta\eta$ to exclude non-flow component are met. Therefore, in order to produce the accurate value of v_n, a different method is adopted. This work defines $q_n = \frac{Q_n}{\sqrt{M}}$, M being the multiplicity of each event in which Q_n is calculated. Then, the following curve is fitted to the frequency distribution of q_n.

$$\frac{dN}{dq_n} = \frac{q_n}{\sigma_n^2} exp\left(-\frac{v_n^2 M + q_n^2}{2\sigma_n^2}\right) I_0 \frac{q_n v_{n\sqrt{M}}}{\sigma_n^2} \tag{6}$$

Here, I_0 is the modified Bessel function of order 0. M and q_n are extracted from the data and feed to the fit; v_n and σ_n are variables determined through the fit, with v_n representing the flow and σ_n accounting for the non-flow component. M and q_n is averaged over each bin of dN/dq_n, which is taken with uniform spacing. To demonstrate the function indeed describes the data, a fit on q_2 over all events is performed.

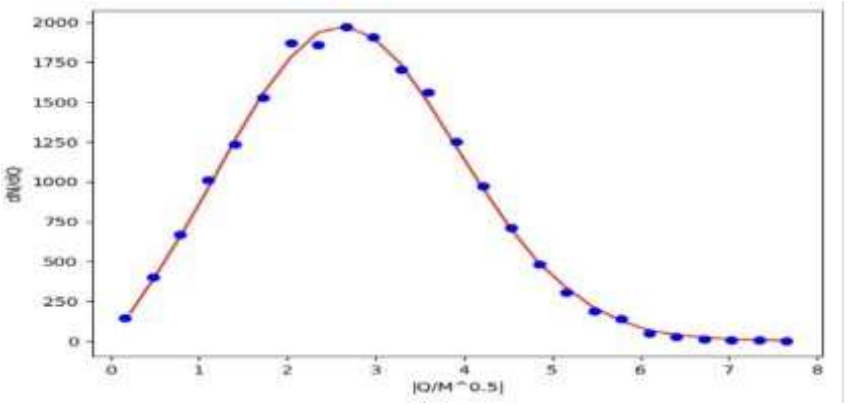

Figure 7. The $q_2 s$ histogram and the curve is compared in this figure. The fit produces σ2 = and v2 = with uncertainty.

DOI: 10.54254/2753-8818/5/20230337

The fit is fairly reasonable considering the uncertainty and graph in Figure 7. However, the same analysis on v_3 or higher yields considerably more statistical uncertainty and therefore is not presented here. As a final step, the fit is performed over each interval of p_T and the results is compared to that from the two-particle correlation method in Figure 8.

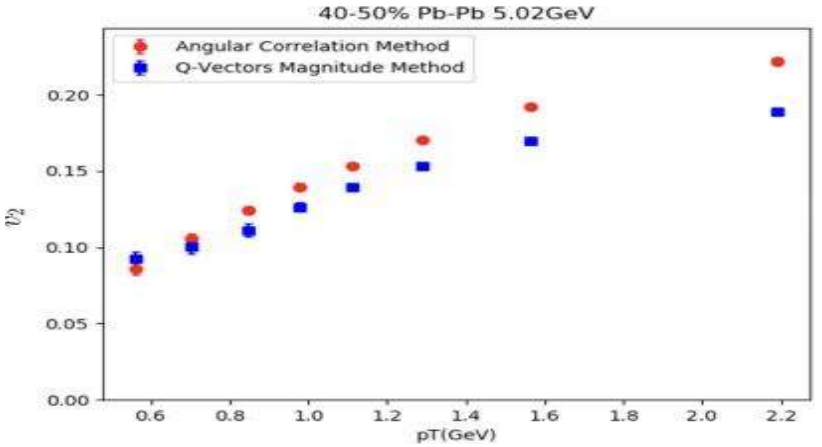

Figure 8. The v_2 distribution determined with Q-vectors and Two Particle Correlations over mid p_T range. The two methods give similar values at lower p_T , but diverges at high p_T . The lower values from the Q-vectors differs from the traditional Q-vector analysis that has higher values.

3.2. Method to analyze jet

Free quarks are sometimes created during the brief existence of the quark-gluon plasma. These quarks zip through the plasma and decompose into a shower of high energy subatomic particles, usually known as jet. In this section, the distribution of jet particles with respect to the event plane is investigated. Due to limitations discussed above, the Two Particles Correlation method does not produce valid result. Therefore, only the Q-vectors method is used here.

This paper has shown that the flow vector angle, ψ, represents the frequency peak of particles in the azimuthal plane. For the analysis here, ψ_2, the peak in elliptical direction, is studied. This elliptical shape inherits from the overlapping part of two nucleus during the collision, as demonstrated in Figure 9a. The frequency peak at $\psi_2$corresponds to the short axis of the ellipse where pressure and acceleration is the greatest.

To determine the distribution with respect to the frequency peak, ψ_2 of each event is subtracted from ϕ of particles in the event. Particles within $\pm\theta$ of the major axis are selected as the “long side” objects, while those within $\pm\theta$ of the minor axis are selected for “short side”, as reflected in Figure 9b.

DOI: 10.54254/2753-8818/5/20230337

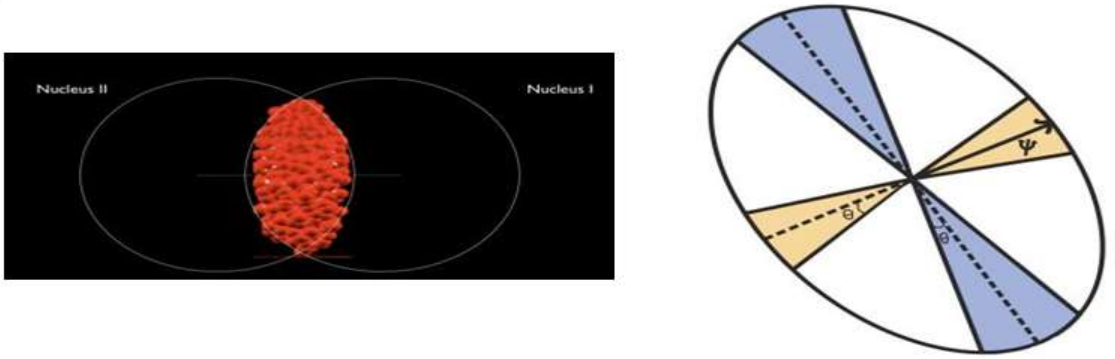

(a) The impact parameter causes the elliptical shape of the plasma
(b) Event plane with Ψ vector and selection angle θ labeled

Figure 9. θ, as labeled in part a, determines the cutoff boundary for the long side (blue) and the short side (yellow) selections.

The Ψ vector corresponds to the minor axis where particle frequency is the highest due to higher pressure.

Next, the q_{2s} of the events are calculated. Upper and lower 20% events in the q_2 histogram are selected. As discussed, this corresponds to selecting events with the highest and lowest elliptical asymmetry. To avoid auto-correlation $p_T < 2GeV$ (non-jet particles) are used in the q_2 calculations.

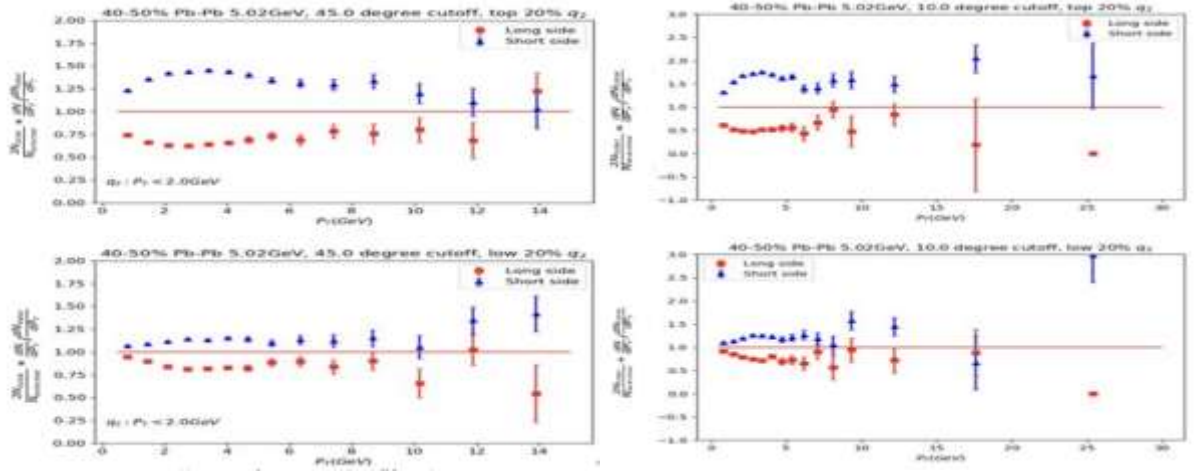

(a) p_T range of 0 to 15 GeV and cutoff θ = 45° (b)p_T range of 0 to 30 GeV and cutoff θ = 10.

Figure 10. Two sets of comparisons between upper and lower 20 % q2 are made in the figures.

In each individual plot, the frequency of the short side and the long side are graphed against each other over a pT range. The y-axis of the graphs are normalized by dividing by total particles in the bin and re-centering around y = 1.

As shown in Fig.10, in both narrow selections ($\theta = 10$) and wide selection ($\theta = 30$), the difference between jet frequency in the short side and the frequency in the long side is smaller in lower 20% compared to upper 20% q_2. Because higher q_2 corresponds to more elliptically shaped plasma, jet particles experience significantly more energy lost when travelling through the long side of a high q_2 plasma. This energy lost decreases p_T and causes the higher difference between long-side frequency and short-side frequency in the upper 20% q_2 selection.

DOI: 10.54254/2753-8818/5/20230337

4. Conclusion

The previous method of CMS analysis using angular correlation between charged particles has been applied to a wide centrality range of PbPb collisions at $\sqrt{s_{NN}} = 5.02T\ eV$. Correlations with large relative pseudorapidity ($2 < |\Delta\eta| < 4$) have been studied as a function of transverse momentum of the collision particles, p_T .The result depicts strong correlation for p_T of middle range $1 < pT < 1.5GeV$, but the correlation does not hold for high or low p_T ranges due to jet fragmentation at near side, $\Delta\phi = 0$, and away side, $\Delta\phi = \pi$, that is unrelated to hydrodynamic flow. The relation is further proven when the analysis from the two different methods converge.

To further quantify the dependence of the correlations on relative azimuthal angle, a Fourier decomposition of the distributions with respect to $\Delta\phi$ was performed and fourier coefficients ($V_{n\Delta}$) are obtained with small statistical error. This implies a very strong connection of the long-range azimuthal dihadron correlations to the single-particle azimuthal anisotropy in heavy ion collisions.

From the Q-vector analysis, one can observe that the frequency of jet is highly dependent on the shape asymmetries of the quark-gluon plasma. The energy lost traveling through the denser side of the plasma is significant enough to decrease the frequency of jet particles in those directions to nearly zero.

The way of quantitatively studying the correlation data presented in this paper provides important inputs to various theoretical models such as the hydrodynamic calculations of higher-order Fourier components.

References

[1] CMS Collaboration. (2011) Long-range and short-range dihadron angular correlations in central Pb Pb collisions at √sNN = 2.76 TeV. JHEP 07, 076

[2] ALICE Collaboration. (2011) Harmonic decomposition of two-particle angular correlations in Pb–Pb collisions at √sNN = 2.76 TeV. https://arxiv.org/pdf/1109.2501.pdf

[3] CMS Collaboration. (2013) Multiplicity and transverse momentum dependence of two- and four-particle correlations in pPb and PbPb collisions. Phys. Lett. B. 724, 213.

[4] CMS Collaboration. (2012) Centrality dependence of dihadron correlations and azimuthal anisotropy harmonics in PbPb collisions at √sNN = 2.76 TeV. Eur. Phys. C. 72, 10052

[5] STAR Collaboration. (2003) Disappearance of back-to-back high pT hadron correlations in central Au+Au collisions at √sNN = 200 GeV. Phys. Rev. Lett. 90, 082302,

[6] STAR Collaboration. (2009) Long range rapidity correlations and jet production in high energy nuclear collisions. Phys. Rev. C. 80, 064912,

[7] STAR Collaboration. (2010) System size dependence of associated yields in hadron-triggered Jets. Phys. Lett. B. 683, 123

[8] STAR Collaboration. (2005) Distributions of charged hadrons associated with high transverse momentum particles in pp and Au+Au collisions at √sNN = 200 GeV. Phys. Rev. Lett. 95,152301

[9] PHENIX Collaboration. (2007) System size and energy dependence of jet-induced hadron pair correlation shapes in Cu+Cu and Au+Au collisions at √sNN = 200 and 62.4 GeV. Phys.Rev. Lett. 98, 232302

[10] PHENIX Collaboration. (2008) Dihadron azimuthal correlations in Au+Au collisions at √sNN = 200 GeV". Phys. Rev. C. 78, 014901

[11] PHOBOS Collaboration. (2010) High transverse Momentum Triggered Correlations over a Large Pseudorapidity Acceptance in Au+Au Collisions at √sNN = 200 GeV. Phys. Rev.Lett. 104, 062301

[12] PHOBOS Collaboration. (2010) System size dependence of cluster properties from twoparticle angular correlations in Cu+Cu and Au+Au collisions at √sNN = 200 GeV. Phys. Rev. C. 81, 024904

[13] P. Christiansen, Computer exercise about elliptic flow (Lund University, 2015).